Stepwise Reduction of Dinitrogen Occurring on a Divanadium Model Compound: A Synthetic, Structural, Magnetic, Electrochemical, and Theoretical Investigation on the $[V{=}N{=}N{=}V]^{n+}$ [$n = 4-6$] Based Complexes

Richard Ferguson,[†,‡] Euro Solari,[‡] Carlo Floriani,*[,‡] Domenico Osella,[§] Mauro Ravera,[§] Nazzareno Re,[⊥] Angiola Chiesi-Villa,[∥] and Corrado Rizzoli[∥]

Contribution from the Institut de Chimie Minérale et Analytique, BCH, Université de Lausanne, CH-1015 Lausanne, Switzerland, Dipartimento di Chimica Inorganica, Chimica Fisica e Chimica dei Materiali, Università di Torino, I-10125 Torino, Italy, Dipartimento di Chimica, Università di Perugia, I-06100 Perugia, Italy, and Dipartimento di Chimica, Università di Parma, I-43100 Parma, Italy

Received April 17, 1997[⊗]

Abstract: This report details an extensive investigation on vanadium−dinitrogen complexes containing the $[V(\mu\text{-}N_2)V]^{n+}$ skeleton with a variable oxidation state of the metal and reduction degree of dinitrogen, n varying from 6 → 5 → 4. This skeleton can be associated to alkali cations in ion-separated or ion-pair tight forms. The reaction of $[(Mes)_3V(thf)]$, **1** [Mes = 2,4,6-$Me_3C_6H_2$], with Lewis acids [$AlPh_3$, $B(C_6F_5)_3$] removed the THF molecule leading under nitrogen to the formation of the diamagnetic complex $[(Mes)_3V(\mu\text{-}N_2)V(Mes)_3]$, **4**. The reaction of **1** with N_2 also occurs under reducing conditions using Na or K metals. As supported by the electrochemical study, the preliminary stage is in both cases the formation of the vanadium(II) desolvated form $[V(Mes)_3]^-$, **5**. The reaction of **5** with N_2 in the case of potassium and in the presence of **1** leads to the compound $\{[(Mes)_3V(\mu\text{-}N_2)V(Mes)_3]^-[K(digly)_3]^+\}$, **11**, which, depending on the reaction conditions, undergoes a further reduction to $[\{K(digly)_3(\mu\text{-}Mes)_2(Mes)V\}_2(\mu\text{-}N_2)]$, **12** [digly = diethylene glycol dimethyl ether]. Similarly, the reduction of **1** with sodium gave, depending on the workup mode, $\{[(Mes)_3V(\mu\text{-}N_2)V(Mes)_3]^{2-}[Na(digly)_2]^+{}_2\}$, **13**, or $\{[(Mes)_3V(\mu\text{-}N_2)(\mu\text{-}Na)V(Mes)_3]^-[Na(digly)_2]^+\}$, **14**, both containing the dianion $[(Mes)_3V(\mu\text{-}N_2)V(Mes)_3]^{2-}$, **8**. Complex **4** releases upon protonation exclusively N_2, while complexes **11**−**14** release N_2, N_2H_4, and NH_3 in amounts depending on the degree of reduction of the dinitrogen and the structure of the complex. The electrochemical reduction of **1** shed light on the intermediate formation of **5** and its conversion to **8**, which was oxidized to the monoanion $[(Mes)_3V(\mu\text{-}N_2)V(Mes)_3]^-$, **7** (which is the precursor of **8** in the chemical reduction). The magnetic studies coupled with the theoretical interpretation are in agreement with the presence of a d^2-d^2 couple in **4**, a d^1-d^1 in **12**−**14**, and a d^1-d^0 in **11**. This, along with the structural studies on **11**−**14**, suggest a cumulenic structure $[V{=}N{=}N{=}V]^{+n}$ [$n = 5, 4$] for **11**−**14**.

Introduction

The metal-assisted activation of dinitrogen is a challenging topic in synthetic chemistry and catalysis.[1] At present, N_2 complexes are known for many transition metals; however, those which promote the reduction of dinitrogen or react in a well-defined manner to give nitrogen-containing compounds are few.[1,2] Metal-mediated N_2 chemistry has proven to be much less manageable and characterizable than the metal-assisted chemistry of the isoelectronic carbon monoxide molecule. Most current research centers on understanding the mechanism for the stepwise reduction of N_2 and the incorporation of N_2 into organic substrates.[1f] An important feature of this chemistry is that N_2 must be polarized before being attacked by an appropriate nucleophile or electrophile. We felt that this polarization of N_2 might be achieved by using either strongly reducing metal or bifunctional systems containing both an electron rich (transition metal ion) and a Lewis acid center, *i.e.*, an alkali cation. The latter can be introduced in the reduction step of the transition metal bound N_2 using alkali metals. The first widely known bifunctional system for converting N_2 into NH_3 and N_2H_4 is based on the vanadium(II)−magnesium(II) couple.[1g,3] Such a bifunctional approach along with the recent discovery of a vanadium-containing nitrogenase[4] prompted us to chose vanadium; also, some rare simple examples of vanadium compounds fixing dinitrogen are actually known.[5]

* To whom correspondence should be addressed.
[†] Present address: Department of Chemistry and Physics, Wagner College, Staten Island, NY 10301.
[‡] Université de Lausanne.
[§] Università di Torino.
[⊥] Università di Perugia.
[∥] Università di Parma.
[⊗] Abstract published in *Advance ACS Abstracts,* October 1, 1997.

(1) (a) Allen, A. D.; Harris, R. O.; Loescher, B. R.; Stevens, J. R.; Whiteley, R. N. *Chem. Rev.* **1973**, *73*, 11. (b) Chatt, J.; Dilworth, J. R.; Richards, R. L. *Chem. Rev.* **1978**, *78*, 589. (c) Henderson, R. A.; Leigh, G. J.; Pickett, C. J. *Adv. Inorg. Chem. Radiochem.* **1983**, *27*, 197. (d) Leigh, G. J. *Acc. Chem. Res.* **1992**, *25*, 177. (e) Leigh, G. J. *New J. Chem.* **1994**, *18*, 157. (f) Hidai, M.; Mizobe, Y. *Chem. Rev.* **1995**, *95*, 1115. (g) Bazhenova, T. A.; Shilov, A. E. *Coord. Chem. Rev.* **1995**, *144*, 69.

(2) Laplaza, C. E.; Johnson, M. J. A.; Peters, J. C.; Odom, A. L.; Kim, E.; Cummins, C. C.; George, G. N.; Pickering, I. J. *J. Am. Chem. Soc.* **1996**, *118*, 8623−8638 and the exhaustive list of references therein.

(3) Luneva, N. P.; Nikonova, L. A.; Shilov, A. E. *Kinet. Katal.* **1980**, *21*, 1041. Shilov, A. E.; Denisov, D. N.; Efimov, O. N.; Shuvalov, V. F.; Shuvalova, N. I.; Shilova, A. K. *Nature (London)* **1971**, *231*, 460. Denisov, N. T.; Efimov, O. N.; Shuvalova, N. I.; Shilova, A. K.; Shilov, A. E. *Zh. Fiz. Khim.* **1970**, *44*, 2694.

(4) George, G. N.; Coyle, C. L.; Hales, B. J.; Cramer, S. P. *J. Am. Chem. Soc.* **1988**, *110*, 4057. Morningstar, J. E.; Hales, B. J. *J. Am. Chem. Soc.* **1987**, *109*, 6854. Robson, R. L.; Eady, R. R.; Richardson, T. H.; Miller, R. W.; Hawkins, M.; Postgate, J. R. *Nature (London)* **1986**, *322*, 388. Arber, J. M.; Dobson, B. R.; Eady, R. R.; Stevens, P.; Hasnain, S. S.; Garner, C. D.; Smith, B. E. *Nature (London)* **1986**, *325*, 372. Bishop, P. E.; Jarlenski, D. M. L.; Hetherington, D. R. *J. Bacteriol.* **1982**, *150*, 1244.

S0002-7863(97)01229-8 CCC: $14.00

We focused our attention on vanadium−aryl compounds, because aryl groups are particularly appropriate as ancillary ligands since they are almost exclusively σ-donor in character, being unable to accommodate electron density from the metal. This strategy has precedents in the area of dinitrogen reduction with low-valent homoleptic aryl−iron compounds. No dinitrogen−iron species have yet been clearly identified.[6]

A second important perspective in using metal−alkyl or −aryl derivatives is the expectation that the polarized -N_2- molecule would participate in migratory insertion reactions like CO, namely, as far as concerns early transition metals.[7] Our model compound [$VMes_3$(THF)][8] (Mes = 2,4,6-$Me_3C_6H_2$) undergoes stepwise reduction to give three different dinitrogen complexes containing the $[V-N-N-V]^{n+}$ skeleton [n = 6, 5, 4]; the degree of N_2 reduction depends on the oxidation state of the metal ion. The electrochemical, theoretical, and magnetic studies will be presented in addition to the synthetic and structural data; such information gives us a better understanding of the electronic configuration of the $[V-N-N-V]^{n+}$ species, which have been isolated in both ion-separated and ion-pair forms. Our initial results have already been communicated.[5d]

Experimental Section

All operations were carried out under an atmosphere of purified nitrogen. All solvents were purified by standard methods and freshly distilled prior to use. Magnetic susceptibility measurements were made on a MPMS5 SQUID susceptometer (Quantum Design Inc.) operating at a magnetic field strength of 1 kOe. Corrections were applied for diamagnetism calculated from Pascal constants.[9] Effective magnetic moments were calculated by the equation $\mu_{eff} = 2.828(\chi T)^{1/2}$ where χ is the magnetic susceptibility per vanadium. Fitting of the magnetic data to the theoretical expression were performed by minimizing the agreement factor, defined as

$$F = \sum_i \frac{[\chi_i^{obsd} T_i - \chi_i^{calcd} T_i]^2}{(\chi_i^{obsd} T_i)^2}$$

through a Levenberg−Marquardt routine.[10]

The synthesis of [V(Mes)$_3$(THF)], **1**, has been performed as reported.[8a]

Analysis for N_2, N_2H_4, and NH_3 for Dinitrogen-Containing Complexes.[11,12] **Reaction of Nitrogen-Containing Compounds with 0.1 M HCl(aq).** A 250 mL two-neck round bottom flask was charged with 100 mL of 0.1 M HCl (NH_3 free) and degassed under N_2. A thin glass vial containing the sample to be analyzed (0.600−1.000 g) was placed in the flask, and the flask was connected to a device for measuring gas evolution. The temperature of the system was adjusted to 15−22 °C. After thermodynamic equilibrium was reached, the vial was broken by a stirring and shaking action, and the volume of N_2 evolved was measured.

The solution containing decomposition products (typically light blue) was filtered and a stock solution (250 mL) prepared with doubly distilled water. A sample was removed, diluted, and on addition of Kovac's reagent, [*p*-(dimethylamino)benzaldehyde],[11] analyzed spectrophotometrically (424, 482 nm) for NH_2NH_2 (note: sample solution must contain between 0.1 and 1 mg/L of hydrazine). The amount of hydrazine was determined from a calibration curve prepared from known hydrazine hydrate concentrations.

A sample, typically 50−100 cm^3, of the stock solution was transferred to a 250 mL distillation apparatus containing a thin glass vial of KOH (*ca*. 1.5 g connected to a receiver flask containing HCl (0.1 M, 100 mL, NH_3 free) (N.B. care was taken to ensure that the receiver arm was submerged beneath the surface of the 0.1 M HCl solution). On reflux the KOH vial was broken by vigorous stirring and the solvent removed to near dryness. The distillate was transferred to a volumetric flask (100 mL) and the NH_3 analyzed spectrophotometrically at 524 nm using Nessler's reagent (N.B. the sample must contain between 0.1 and 1 mg/L of NH_3). Concentrations were determined from a calibration curve prepared from an NH_4Cl stock solution.

Synthesis of 3. A toluene (300 mL) suspension of **1** (5.66 g, 11.7 mmol) was added to a toluene suspension of $AlPh_3$ (3.0 g, 11.7 mmol) at −30 °C. The suspension was warmed up to room temperature to give a brown solution. Then the solution was evaporated to dryness and the solid collected and washed several times with *n*-hexane (90%). Anal. Calcd for **3**, $[V(Mes)_3]_n$, $C_{27}H_{33}V$: C, 79.41; H, 8.08. Found: C, 78.97; H, 8.27. μ_{eff} = 2.25 BM at 298 K.

Synthesis of 4, Method A. To a toluene (200 mL) solution of **1** (2.05 g, 4.26 mmol) at −60 °C was added $B(C_6F_5)_3$ (2.20 g, 4.30 mmol). The temperature was raised to 0 °C and the mixture stirred for 2 days under 1−2 atm of N_2. The resulting orange microcrystalline product (pyrophoric) collected by filtration at −10 °C and dried *in vacuo* (65%). Anal. Calcd for **4**, $C_{54}H_{66}N_2V_2$: C, 76.76; H, 7.82; N, 3.32. Found: C, 77.13; H, 7.88; N, 3.88. Reaction of **4** with THF liberates N_2 to give the blue color of **1**. Complex **4** is diamagnetic.

Synthesis of 4, Method B. To a toluene (400 mL) suspension of **1** (4.96 g, 10.3 mmol) at −30 °C was added $AlPh_3$ (2.69 g, 10.4 mmol). The suspension was stirred at room temperature for 12 h to give a solution from which **4** precipitated as a brown microcrystalline solid (75%). Anal. Calcd for $(Mes)_3VNNV(Mes)_3$, $C_{54}H_{66}N_2V_2$: C, 76.76; H, 7.82; N, 3.32. Found: C, 76.92; H, 7.89; N, 3.18.

Synthesis of 9. A 500 mL two-neck round bottom flask was charged with 200 mL of diglyme and degassed under Ar. **1** (4.09 g, 8.49 mmol) was added, followed by a large excess (0.43 g, 18.7 mmol) of sodium sand. The mixture was stirred vigorously at room temperature for 2 h under Ar. The color changed from blue to violet to brown. The mixture was filtered to eliminate excess Na (no other solid was found in the filter, in contrast to the reaction under N_2). The filtrate was concentrated under vacuum down to 50 mL. At room temperature, a microcrystalline material precipitated and was collected by filtration at 0 °C. The product was washed with Et_2O (50 mL), yielding a light purple, microcrystalline solid (air/H_2O sensitive) (50%). The second product, **10**, "V(Mes)$_2$", was not isolated or characterized. Anal. Calcd for **9**, $C_{48}H_{72}NaO_6V$: C, 70.41; H, 8.80. Found: C, 70.23; H, 8.37.

Synthesis of 11. Diglyme (100 mL) and **1** (4.37 g, 9.09 mmol) were combined in a 1000 mL two-neck round bottom flask. The temperature was lowered to 0 °C, and then a ball of potassium metal (0.35 g, 8.95 mmol−excess) was added. The partial N_2 pressure was raised to 1−2 atm and the mixture stirred vigorously for 18 h, resulting in a black color. Filtration of the product mixture at −5 °C yielded a microcrystalline black solid and any excess K, which was removed.

(5) (a) Song, J.-I.; Berno, P.; Gambarotta, S. *J. Am. Chem. Soc.* **1994**, *116*, 6927. (b) Berno, P.; Hao, S.; Minhas, R.; Gambarotta, S. *J. Am. Chem. Soc.* **1994**, *116*, 7417. (c) Buijink, J.-K. F.; Meetsma, A.; Teuben, J. H. *Organometallics* **1993**, *12*, 2004. (d) Ferguson, R.; Solari, E.; Floriani, C.; Chiesi-Villa, A.; Rizzoli, C. *Angew. Chem., Int. Ed. Engl.* **1993**, *32*, 396. (e) Rehder, D.; Woitha, C.; Priebsch, W.; Gailus, H. *J. Chem. Soc., Chem. Commun.* **1992**, 364. (f) Woitha, C.; Rehder, D. *Angew. Chem., Int. Ed. Engl.* **1990**, *29*, 1438. (g) Leigh, G. J.; Prieto-Alcón, R.; Sanders, J. R. *J. Chem. Soc., Chem. Commun.* **1991**, 921. (h) Edema, J. J. H.; Meetsma, A.; Gambarotta, S. *J. Am. Chem. Soc.* **1989**, *111*, 6878.

(6) Some significant precedents in the use of low-valent homoleptic iron−aryl compounds in dinitrogen reduction exist, though no iron−dinitrogen species has been yet clearly identified: (a) Shilov, A. E. *New J. Chem.* **1992**, *16*, 213 and references therein. (b) Bazhenova, T. A.; Kachapina, L. M.; Shilov, A. E. *J. Organomet. Chem.*, **1992**, *428*, 107. (c) Shilov A. E. In *Perspectives in Coordination Chemistry*; Williams, A. F., Floriani, C., Merbach, A., Eds.; VCH, Weinheim: 1992; p 233.

(7) Durfee, L. D.; Rothwell, I. P. *Chem. Rev.* **1988**, *88*, 1059 and references therein.

(8) (a) Vivanco, M.; Ruiz, J.; Floriani, C.; Chiesi-Villa, A.; Rizzoli, C. *Organometallics* **1993**, *12*, 1794. (b) Vivanco, M.; Ruiz, J.; Floriani, C.; Chiesi-Villa, A.; Rizzoli, C. *Organometallics* **1993**, *12*, 1802. (c) Ruiz, J.; Vivanco, M.; Floriani, C.; Chiesi-Villa, A.; Rizzoli, C. *Organometallics* **1993**, *12*, 1811.

(9) Boudreaux, E. A.; Mulay, L. N. In *Theory and application of Molecular paramagnetism*; Wiley: New York, 1976; pp 491−495.

(10) Press, W. H., Flannery, B. P.; Teukolsky, S. A.; Vetterling, W. T. *Numerical Recipes;* Cambridge University Press: Cambridge, 1989.

(11) Thomas, L. C.; Chamberlain, G. J. *Colorimetric Chemical Analytical Methods*, 9th ed.; Wiley: New York, 1980; p 193.

(12) *Vogel's Textbook of Quantitative Chemical Analysis*, 5th ed.; Longman: London, 1989; p 679.

Table 1. Experimental Data for the X-ray Diffraction Studies on Crystalline Complexes **11**−**14**[a]

compd	**11**	**12**	**13**	**14**
formula	$C_{54}H_{66}N_2V_2{\cdot}C_{18}H_{42}KO_9$	$C_{66}H_{94}K_2N_2O_6V_2{\cdot}0.6667C_4H_{10}O$	$C_{54}H_{66}N_2V_2{\cdot}2C_{12}H_{28}NaO_6{\cdot}0.5C_4H_8O$	$C_{54}H_{66}N_2NaV_2{\cdot}C_{12}H_{28}NaO_6{\cdot}C_6H_6$
a =	23.322(8)	40.222(2)	16.376(4)	11.823(4)
b =	13.250(3)	40.222(2)	21.782(5)	21.651(2)
c =	25.944(9)	14.348(4)	25.472(6)	28.696(6)
α =	90	90	90	90
β =	116.50(1)	90	92.18(2)	90
γ =	90	120	90	90
V =	7175(4)	20153(6)	9079(4)	7346(3)
Z =	4	9	4	4
fw	1286.6	1241.0	1463.7	1237.5
space group	$P2_1/n$ (No. 14)	$R\bar{3}$ (No. 148)	$P2_1/n$ (No. 14)	$C222_1$ (No. 20)
t =	−97	22	22	22
λ =	0.71069	1.54178	1.54189	1.54178
ρ_{calc} =	1.191	0.920	1.071	1.119
μ =	3.61	29.06	22.37	26.24
transmission coeff	0.985−1.000	0.902−1.000	0.562−1.000	0.861−1.000
R =	0.048	0.081	0.085	0.045 [0.060][a]
wR2 =	0.101	0.272	0.272	0.138 [0.168]
GOF =	1.047	0.897	0.878	0.779

[a] $R = \Sigma|\Delta F|/\Sigma|F_o|$. wR2 = $[\Sigma(w(\Delta F^2)^2/\Sigma(wF_o^2)^2]^{1/2}$. GOF = $[\Sigma w|\Delta F|^2/(NO - NV)]^{1/2}$. Values in square brackets refer to the "inverted structure".

The product was dried *in vacuo* (89%) and stored at 4 °C. X-ray quality crystals of **11** were obtained as follows: a solution of **11** (5.20 g) in benzene (50 mL) was filtered at 5 °C and dried *in vacuo*. This purified product (1.65 g) was then redissolved in benzene (45 mL) and filtered at 40 °C, and the filtrate was cooled to 5 °C over 3 days. The resulting black crystals were collected by filtration at 5 °C. Anal. Calcd for **11**, $C_{72}H_{108}KN_2O_9V_2$: C, 67.21; H, 8.46; N, 2.18. Found: C, 67.74; H, 8.53; N, 2.58.

Synthesis of 12. To a toluene (200 mL) solution of **1** (4.32 g, 8.99 mmol) at 0 °C was added a ball of K (0.35 g, 8.98 mmol), and the partial N_2 pressure was raised to 1−2 atm. After 18 h of vigorous stirring, the color had changed from blue to orange-brown. Diglyme (3 mL) was added to the product mixture, and stirring was continued for 10 min at room temperature. The reaction mixture was concentrated *in vacuo* to 10 mL, and then diethyl ether (150 mL) was added. The flask was briefly shaken and left for 3 h, resulting in a black crystalline product. This was then collected by filtration and dried *in vacuo* (69%) and the product stored in the refrigerator. **Making Crystals Suitable for X-ray Structure Determination.** During the preparation, after addition of the diglyme, the solution was concentrated to 30 mL (instead of 10 mL). Diethyl ether (200 mL) was then added, the flask was shaken and left to stand for 1 h; then the mixture was filtered at room temperature. The filtrate was left in a refrigerator at 4 °C for 2 days. The resulting black crystals were collected by filtration at 4 °C. The reaction yields the same product (plus unconsumed $[V(Mes)_3]$) when carried out with 0.5 equiv of K. Anal. Calcd for **12**·0.7Et_2O, $C_{66}H_{94}K_2N_2O_6V_2{\cdot}0.7C_4H_{10}O$: C, 66.53; H, 7.95; N, 2.35. Found: C, 66.54; H, 8.13; N, 2.48.

Synthesis of 13. To a THF (100 mL) solution of **1** (2.91 g, 6.05 mmol) at 0 °C were added four equally sized pieces of Na (0.14 g, 6.05 mmol). The partial N_2 pressure was raised to 1−2 atm by pinching the N_2 bubbler line before closing the stopcock of the flask. The mixture was stirred vigorously for 10 h, and the color changed from blue to brown. Diglyme (50 mL) was added to the mixture, resulting in the formation of a black microcrystalline solid. This was collected by filtration, washed with diethyl ether (50 mL), dried *in vacuo* (88%), and stored at 4 °C. **Making Crystals Suitable for X-ray Structure Determination.** Approximately 6.0 g of product was combined with THF (45 mL) in a 250 mL two-neck round bottom flask. The mixture was filtered at room temperature, and the filtrate was slowly cooled to −35 °C over 1 week. The black crystals were collected by filtration at −35 °C. Anal. Calcd for **13**·0.5THF, $C_{80}H_{126}N_2Na_2O_{0.5}V_2$: C, 65.62; H, 8.61; N, 1.96. Found: C, 65.34; H, 8.64; N, 1.49.

Synthesis of 14. To a diglyme (100 mL) solution of **1** (2.80 g, 5.82 mmol) was added a sodium ball (0.12 g, 5.22 mmol). The partial N_2 pressure was raised to 1−2 atm by pinching the N_2 bubbler line before closing the stopcock of the flask. The mixture was stirred vigorously for 2.5 days at *ca*. 20 °C, resulting in a color change from blue to black-brown. Filtration of the product mixture yielded a shiny black solid, which was washed with benzene (100 mL) at room temperature and dried *in vacuo* (96%) (note that Na is the limiting reagent to avoid contamination of product by Na). The product was stored at 4 °C. **Making Crystals Suitable for X-ray Structure Determination. 14** (2.65 g) and benzene (100 mL) were combined in a 250 mL two-neck round bottom flask. The mixture was briefly shaken, and then the bottom quarter of the flask was immersed in an oil bath at *ca*. 65 °C; the mixture was left to convect for 2 h. The heating element was disengaged, and when the oil bath had reached room temperature, the black crystals were collected by decantation. The reaction gave the same product (plus unconsumed **1**) when carried out with 0.5 equiv of Na. Anal. Calcd for **14**, $C_{66}H_{94}N_2Na_2O_6V_2$: C, 68.38; H, 8.17; N, 2.42. Found: C, 68.15; H, 8.01; N, 2.71.

X-ray Crystallography for Complexes 11−**14.** Crystal data and details associated with data collection are given in Tables 1 and S1. Data were collected on a single-crystal diffractometer (Enraf-Nonius CAD4 for **11**, Rigaku AFC6S for **12**−**14**) at 178 K for **11** and at 295 K for **12**−**14**. For intensities and background, individual reflection profiles[13] were analyzed. The structure amplitudes were obtained after the usual Lorentz and polarization corrections, and the absolute scale was established by the Wilson method.[14] The crystal quality was tested by ψ scans showing that crystal absorption effects could not be neglected. The data were corrected for absorption using a semiempirical method[15] for all the complexes. The function minimized during the least-squares refinement was $\Delta w(\Delta F^2)^2$. Weights were applied according to the scheme $w = 1/[\sigma^2(F_o^2) + (aP)^2]$ ($P = (F_o^2+2F_c^2)/3$ and a = 0.0548, 0.1516, 0.1169, and 0.0623, for complexes **11**−**14**, respectively. Anomalous scattering corrections were included in all structure factor calculations.[16b] Scattering factors for neutral atoms were taken from ref 16a for non-hydrogen atoms and from ref 17 for H. Among the low-angle reflections no correction for secondary extinction was deemed necessary.

All calculations were carried out on an IBM PS2/80 personal computer and on an ENCORE 91 computer. The structures were solved by the heavy-atom method starting from three-dimensional Patterson maps using the observed reflections. Structure refinements were carried

(13) Lehmann, M. S.; Larsen, F. K. *Acta Crystallogr. Sect. A: Cryst. Phys., Diffr., Theor. Gen. Crystallogr.* **1974**, *A30*, 580.
(14) Wilson, A. J. C. *Nature* **1942**, *150*, 151.
(15) North, A. C. T.; Phillips, D. C. Mathews, F. S. *Acta Crystallogr. Sect. A: Cryst. Phys., Diffr., Theor. Gen. Crystallogr.* **1968**, *A24*, 351.
(16) (a) *International Tables for X-ray Crystallography*; Kynoch Press: Birmingham, England, 1974; Vol IV, p 99. (b) Reference 16a, p 149.
(17) Stewart, R. F.; Davidson, E. R.; Simpson, W. T. *J. Chem. Phys.* **1965**, *42*, 3175.

out using SHELXL92[18] and based on the unique observed data for **11** and on the unique total data for **12**−**14**.

During the refinements the aromatic rings of complexes **12**−**14** were constrained to be regular hexagons (C−C 1.39(1) Å), while the C−C and C−O bond distances of the diglyme molecule in **12** and of the THF molecule of crystallization in **13** were constrained to be 1.54(1) and 1.48(1) Å, respectively. The hydrogen atoms, except those related to the solvent molecules of crystallization in **12** and **13**, which were ignored, were located from difference Fourier maps for **11** and put in geometrically calculated positions for **12**−**14**. They were introduced in the subsequent refinements as fixed atom contribution with *U*'s fixed at 0.05 for **11**, 0.12 for **14**, and 0.15 Å^2 for **12** and **13**. The final difference maps showed no unusual feature, with no significant peak above the general background. The crystal chirality of complex **14**, which crystallizes in a polar space group, was tested by inverting all the coordinates ($x, y, z \mid -x, -y, -z$) and refining to convergence once again. The resulting *R* values quoted in Table 1 indicated that the original choice should be considered the correct one.

Crystal data are listed in Table S1 and final atomic coordinates in Tables S2−S5 for non-H atoms and in Tables S6−S9 for hydrogens. Thermal parameters are given in Tables S10−S13 and bond distances and angles in Tables S14−S17.

Electrochemistry. Electrochemical measurements were performed using an EG&G PAR 273 electrochemical analyzer interfaced to a personal computer, employing PAR M270 Electrochemical Software. A standard three-electrode cell was designed to allow the tip of the reference electrode to closely approach the working electrode. The cell was enclosed in a drybox. All measurements were carried out under Ar or N_2 in anhydrous deoxygenated THF. Solutions were 1×10^{-3} M with respect to the compounds under study and 2×10^{-1} M with respect to the supporting electrolyte, $NaBPh_4 \times 2$triglyme. The working electrode was a Pt disk (diameter = 1 mm) sealed in soft glass which was polished with alumina. The reference electrode was a AgCl-coated silver wire dipped in a 2×10^{-1} M solution of $NaBPh_4 \times 2$ triglyme in THF and separated from the cell solution by a fine frit. At the end of each experiment, the potential of the Fc/Fc^+ couple was measured *vs* the pseudo-reference electrode and then *vs* an aqueous SCE, to which all data are referred. Under the actual experimental conditions the Fc/Fc^+ couple is located at +0.405 V *vs* SCE. Since the resistence of such a THF solution was exceptionally high, albeit positive feedback *iR* compensation, some potential distortions were observed. This led to higher values of the peak-to-peak separation, ΔE_p. Therefore in all experiments we compared the ΔE_p of the peak couples under study to that of Fc/Fc^+, added as internal standard. Any deviation from the ΔE_p value of 70 mV, assumed to be the constant value of Fc/Fc^+ couple at all scan rates, is taken as an indication of uncompensed *iR* drop and computated as a factor of correction. Therefore, the statement *Nernstian* throughout this work indicates a redox process as reversible as the oxidation of Fc is.[19]

The number of electrons transferred (*n*) in a particular redox process was determined by controlled potential coulometry at a Pt gauze; all experiments were done in duplicate.

Results and Discussion

A. Synthesis. Electron-rich vanadium(III) derivatives are good candidates for dinitrogen fixation, provided the appropriate choice of reaction conditions is made. The parent compound $[V(Mes)_3(thf)]$, **1**, we examine here is completely unreactive toward N_2; however, when the THF molecule is removed using an appropriate Lewis acid, the metal center reacts by either oligomerizing (under Ar), **3**, or binding N_2 (under nitrogen), **4** (Scheme 1).

The nature of the Lewis acid is crucial for the occurrence of the reaction and largely determines the relative yields of products **3** and **4**. Although some boron derivatives, such as $[B(C_6F_5)_3]$,

Scheme 1

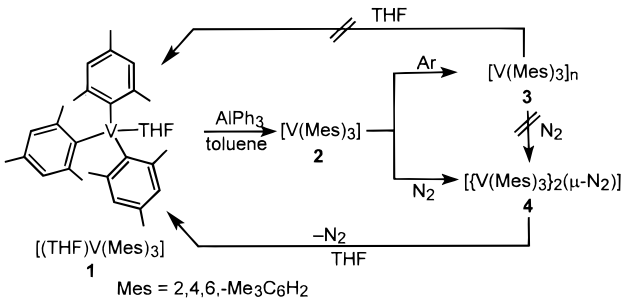

Scheme 2

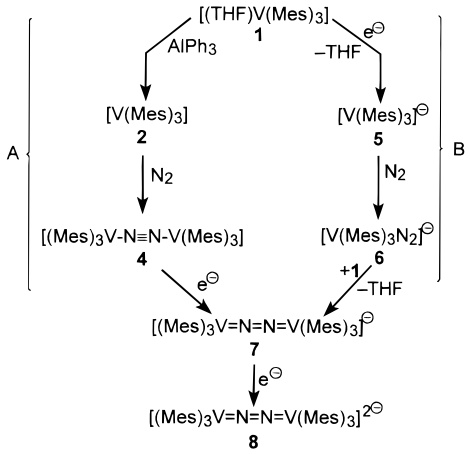

were active, the most effective and less time consuming from a synthetic point of view were the trialkyl or triaryl aluminum species; $AlPh_3$ gave the best yield of **4**. The effectiveness of the Lewis acid is not dependent on its intrinsic Lewis acidity but on its solubility. This is understandable if we compare the very low yield of **4** when using AlR_3 [R = Me or Et] with the higher yield when using $AlPh_3$. The slight solubility of $AlPh_3$ allows a slow delivery of the active species $[V(Mes)_3]$, **2** (Scheme 2), compatible with the low concentration of N_2 in toluene, though some amount of **2** untrapped by N_2 evolves to give **3**. Complex **3** does not react with N_2. Formation of **3** becomes predominant when the reaction in Scheme 1 is carried out using AlR_3 [R = Me, Et]. Both of these Lewis acids are soluble in toluene, quickly giving rise to a high concentration of **2**, which cannot be stabilized as **4** by the low concentration of N_2. The generation of an N_2-active species should occur roughly at the same rate as dinitrogen is supplied to the solution. Carrying out reaction 1 under Ar resulted only in **3**. In the absence of any X-ray analysis, we are not in the position to propose a plausible structure for **3**, whose formulation corresponds to $[V(Mes)_3]_n$, without any solvent. The protonation of **4** with HCl, a standard test for the presence of reduced forms of dinitrogen (NH_3, N_2H_4), gave exclusively N_2 (see Experimental Section). This was not entirely surprising since no reduced N_2 was found in the literature complex $\{[Me_3CCH_2)_3V]_2(\mu\text{-}N_2)\}$ either.[5c] Complex **4** releases N_2 when treated with THF, while the oligomeric form **3** does not go back to **1** under the same conditions.

The access to reduced, activated forms of dinitrogen followed two synthetic routes, using either **1** or **4** as starting materials. The two pathways A and B are shown in Scheme 2.

In both pathways we must remove the THF on vanadium. This was done by using a Lewis acid (pathway A) or reducing the metal (pathway B). Although pathway A appears more logical on paper, it is pathway B which is more practical, since the transformation of **1** into **2**, and then **4**, using a Lewis acid

(18) Sheldrick, G. SHELXL92: Program for Crystal Structure Refinement; University of Göttingen: Göttingen, Germany, 1992.

(19) (a) Connelly, N. G.; Geiger, W. E. *Adv. Organomet. Chem.* **1984**, *23*, 1. (b) Geiger, W. E. In *Organometallic Radical Processes*; Trogler, W. C., Ed.; Elsevier: Amsterdam, 1990.

Scheme 3

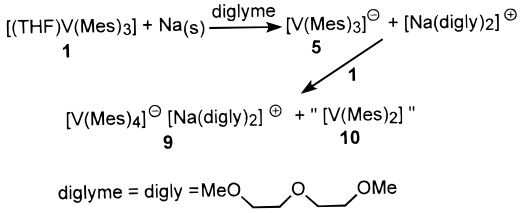

Scheme 4

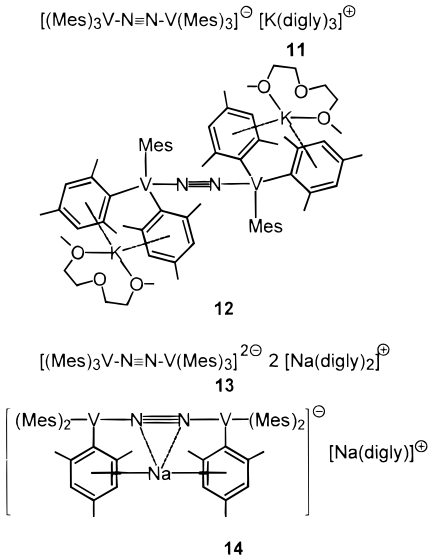

requires two steps instead of one. The electron-rich vanadium(II) in **5** loses THF easily, and a coordination site becomes available for N_2, to give **6**. The reduction is carried out in the presence of N_2, which acts as the stabilizing agent for **5**. In the absence of N_2 (reaction under Ar) **5** is not stable and reacts with **1**, resulting in a ligand disproportionation reaction (Scheme 3).

The enhanced basicity of metal-bonded N_2 in **6** (Scheme 2) allows the displacement of THF from **1** to give **7**, which is further reduced to **8**. Although the sequences (pathways A and B) in Scheme 2 show all the probable intermediates, the syntheses of compounds **4**, **7**, and **8** were all carried out starting from **1**, and not following the sequence **4** → **7** → **8**. Interestingly, the degree to which **1** was reduced to **7** or **8** depended only on the nature of the alkali cation and the solvent conditions, not on how much alkali metal was used.

The reaction of **1** with potassium metal in a V/K = 1 molar ratio in diglyme gave **11** (Scheme 4), containing the monoanion **7**, and $[K(digly)_3]^+$ as countercation. When the reaction was carried out in THF followed by the crystallization from diglyme, we obtained **12**, containing the dianion **8**, and two $[K(digly)]^+$ cations in a tight ion-pair form. Thus, regardless of the V:K stoichiometric ratio, the solvent helps to determine both the degree of N_2 reduction in the dinuclear skeleton and the occurrence of **11** as an ion-separated molecule, or **12** as an ion-pair form. Such solvent structure dependence was also observed in the case of Na metal, though only the dielectronic reduction of the [V(III)−N_2−V(III)] skeleton occurred. The reduction in THF, followed by the addition of diglyme, gave the ion-separated form **13** (Scheme 4). When the reaction was carried out in diglyme the ion-pair **14** was isolated (Scheme 4).

The main question arising at this point was how much is the dinitrogen reduced in complexes **4** and **11**−**14**, namely, in the anions **7** and **8**, as a function of the degree of oxidation of the $[V-N_2-V]^{n+}$ skeleton [n = 6, 5, 4]. The most common chemical test for the presence of reduced N_2 is the reactivity of the metal-bonded N_2 with electrophiles[1a] such as H^+ in the protonolysis reaction.[1d] We used the protonolysis reaction to test our complexes, but we note that the figures we obtained undoubtedly underestimate the reduction degree of dinitrogen due to the presence of the proton sensitive aryl group at the metal.

Table 2

compd	yield of N_2, %	yield of N_2H_4, %	yield of NH_3, %	total, %
4	98			98
11	66	20	7	93
12	42	38	21	101
13	53	27	21	101
14	49	36	11	96

Protonation of **4** and **11**−**14** was carried out with aqueous HCl (0.1 M) at 15−22 °C, and the amounts of N_2, N_2H_4, and NH_3 obtained (Table 2) were analyzed as reported in the Experimental Section. Protonation of **11**−**14** under nonaqueous conditions in THF with dry HCl gave the same results. Some interesting conclusions can be drawn from these data if one assumes that the principal route to free N_2 is *via* protonation of the V−C bonds and to N_2H_4 and NH_3 by protonation of N_2. The yield of N_2 is 100% in the case of **4** due to the low electron density on the unreduced nitrogen atoms; protonation of the more basic carbon of the V−C bond is preferred. In the case of **11**, protonation of both carbon and nitrogen atoms occurs. The N/C protonation ratio increases with compounds **11** through **14**, because of the presence of reduced dinitrogen. Within this sequence we can make some interesting observations. The yields of N_2 from **13** and **14** are roughly the same for these equally reduced species; on the other hand, the N_2H_4/NH_3 ratio is greater for **14**, possibly because the μ-N_2−Na moiety in **14** acts as a template for the production of N_2H_4. The yield of N_2 is the least for **12**, possibly because the two K^+ partially block the protonation site of the V−C bonds, thereby further favoring the protonation of N_2 to give N_2H_4 and NH_3.

Although the protonation of dinitrogen in **11**−**14** has as a competing reaction the protonation of the mesityl groups, the yield of NH_3 and N_2H_4, with respect to **12** and **13**, is higher than expected if one considers the number of electrons exceeding the vanadium(III) oxidation state. This fact is particularly relevant and in agreement with the evidence that, as is true for **11**−**14**, we are not dealing anymore with $[V(III)-N_2-V(III)]^{-n}$ [n = 1, 2] systems but, when n extra electrons are added to **4**, with vanadium(IV) systems (*vide infra*). This implies that the protonation of **11**−**14** should produce not only vanadium(III) but also some vanadium(IV) in order to account for the excess of NH_3 and N_2H_4 derived from **12** and **13**.

B. Structural Studies. First, we will describe the overall structure of each complex in the series **11**−**14**, followed by a conclusive comparison of the structural parameters related to the common V−N−N−V skeleton.

The structure of **11** is determined by the packing of anions **7** (Figure 1) and $[K(digly)_3]^+$ cations in the molar ratio 1/1. A selection of bond lengths and angles is reported in Table 3. The dihedral angles formed by the V1−N1 and V2−N2 lines with the normal to the mean plane through the σ-bonded carbon atoms around V1 and V2 are 11.0(1) and 6.8(2)°, respectively. The vanadium atoms are displaced from their coordination basal planes by 0.543(1) and 0.416(1) Å for V1 and V2, respectively. The V−C bond distances are affected by the charge of the complex, being significantly shorter [average: 2.085(12) Å] than those found in complex **13** [average: 2.189(11) Å] (Table 3).

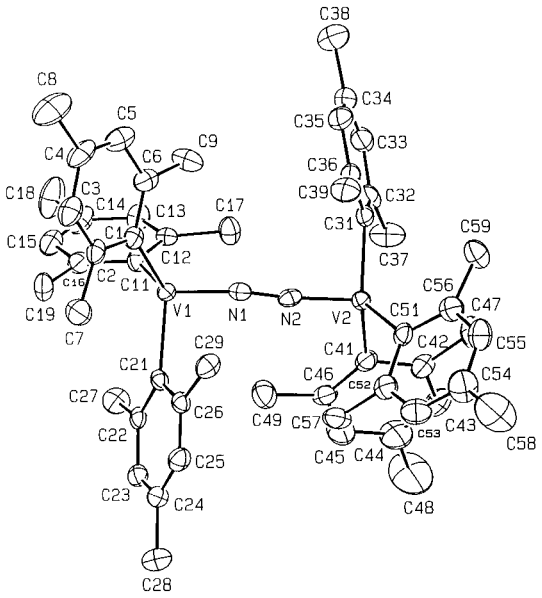

Figure 1. ORTEP drawing of the anion in complex **11** (80% probability ellipsoids).

Table 3. Selected Bond Distances (Å) and Angles (deg) for Complexes **11** and **13**

	11	**13**
V1−N1	1.770(3)	1.775(5)
V1−C1	2.117(3)	2.185(5)
V1−C11	2.076(3)	2.195(5)
V1−C21	2.106(3)	2.171(5)
V2−N2	1.741(3)	1.750(6)
V2−C31	2.112(3)	2.164(5)
V2−C41	2.051(3)	2.238(5)
V2−C51	2.087(3)	2.175(6)
N1−N2	1.222(4)	1.225(7)
C11−V1 −C21	114.4(1)	123.5(2)
C1−V1 −C21	120.7(1)	112.0(3)
C1−V1−C11	105.3(1)	102.6(2)
N1−V1−C21	95.4(1)	102.0(2)
N1−V1−C11	105.0(1)	110.2(2)
N1−V1−C1	115.0(1)	105.3(2)
C41−V2−C51	105.9(1)	101.2(2)
C31−V2−C51	125.2(1)	113.2(2)
C31−V2−C41	117.0(1)	122.0(2)
N2−V2−C51	104.9(1)	104.8(3)
N2−V2−C41	106.0(1)	115.1(3)
N2−V2−C31	94.6(1)	99.7(2)

The structure of **12** is shown in Figure 2, and a selection of bond lengths and angles is reported in Table 4. The structure consists of $[\{K(digly)_3(\mu\text{-}Mes)_2(Mes)V\}_2(\mu\text{-}N_2)]$ centrosymmetric molecules and Et_2O solvent molecules of crystallization in the molar ratio 3/2. The complex molecule possesses a crystallographically imposed inversion center at the midpoint of the N−N bond (Figure 2). A comparison with complexes **11** and **13** shows that the C1···C6 and C11···C16 mesityl rings are slightly rearranged, giving rise to a cavity which accommodates the potassium cation. The two rings are in an "eclipsed" conformation as seen from the torsion angles quoted in Table 5. The potassium cation completes its coordination through three oxygen atoms from a diglyme molecule.

The structure of **13** consists of dianion **8** (Figure 3), $[Na(digly)_2]^+$ cations, and THF solvent molecules of crystallization in the molar ratio 1/2/0.5. A selection of bond lengths and angles is reported in Table 3. The dihedral angles formed by the V1−N1 and V2−N2 lines with the normal to the mean plane through the corresponding σ-bonded carbon atoms are 4.6(2) and 9.1(2)°, respectively. The V−C bond distances are in agreement with those observed in complex **14** (Tables 3 and 4).

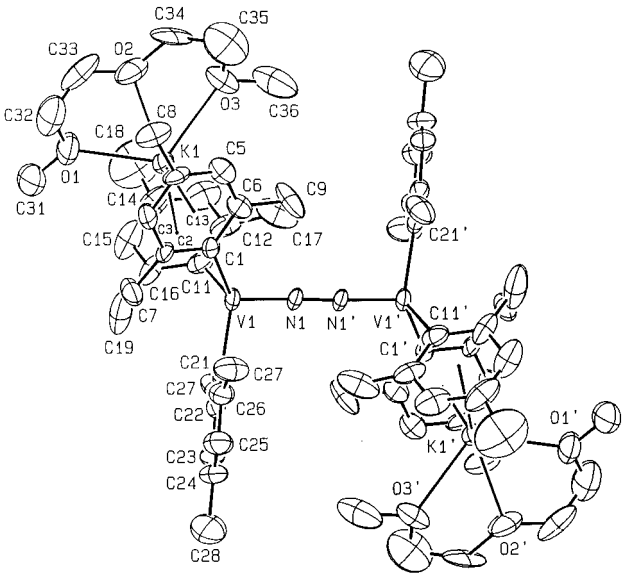

Figure 2. ORTEP drawing of complex **12** (20% probability ellipsoids). Prime denotes a transformation of $1 - x, -y, 1 - z$.

Table 4. Selected Bond Distances (Å) and Angles (deg) for Complexes **12** and **14**

(a) Within the $[\{V(Mes)_3\}_2\text{-}\mu\text{-}(N_2)]$ Units

	12	**14**
V1−N1	1.744(6)	1.757(6)
V1−C1	2.139(11)	2.123(9)
V1−C11	2.110(11)	2.172(9)
V1−C21	2.12(2)	2.193(9)
N1−N1′	1.233(8)	1.271(8)
C11−V1−C21	118.5(5)	118.9(4)
C1−V1−C21	122.1(4)	113.7(4)
C1−V1−C11	96.8(5)	105.4(4)
N1−V1−C21	99.7(4)	92.4(3)
N1−V1−C11	110.4(4)	119.5(4)
N1−V1−C1	109.5(4)	106.7(5)
V1−N1−N1′	178.3(8)	174.7(10)

(b) Within the K1 Coordination Sphere in Complex **12**

K1−O1	2.703(12)	K1−C6	3.175(8)
K1−O2	2.717(20)	K1−C11	3.218(15)
K1−O3	2.805(20)	K1−C12	3.179(14)
K1−C1	3.178(12)	K1−C13	3.300(15)
K1−C2	3.362(12)	K1−C14	3.454(11)
K1−C3	3.535(9)	K1−C15	3.491(18)
K1−C4	3.534(7)	K1−C16	3.376(20)
K1−C5	3.358(10)		

(c) Within the Na1 Coordination Sphere in Complex **14**

Na1−N1	2.513(12)	Na1−C21′	2.570(17)
Na1−N1′	2.607(12)	Na1−C22′	2.388(17)
Na1−C21	2.585(17)	Na1−C23′	2.601(16)
Na1−C26	2.492(17)		

The structure of **14** consists of dimeric $[(Mes)_3V(\mu\text{-}N_2)(\mu\text{-}Na)V(Mes)_3]^-$ anions (Figure 4), $[Na(digly)_2]^+$ cations, and benzene solvent molecules of crystallization in the molar ratio of 1/1/1. A selection of bond lengths and angles is reported in Table 4.

The anion has an imposed crystallographic C_2 symmetry (Figure 4), a dinitrogen molecule linearly bridging two adjacent $[V(Mes)_3]$ units. [V1−N1−N1′, 174.7(10)°]. Coordination around vanadium can be described as a flattened trigonal pyramid with vanadium lying 0.597(3) Å from the plane of the three σ-bonded carbon atoms toward the nitrogen atom (Table 5). The dihedral angle formed by the V1−N1 line with the

Table 5. Comparison of Structural Parameters within the $V(Mes)_3$ Units for Complexes **11**−**14**[a]

	11	**12**	**13**	**14**
(a) Within each $V(Mes)_3$ Unit				
Distances of Vanadium from the Mesityl Rings (Å)				
dist of V1 from C1..C6 plane	0.333(1)	0.217(3)	0.028(1)	0.126(2)
dist of V1 from C11..C16 plane	0.033(1)	0.324(4)	0.139(1)	0.067(3)
dist of V1 from C21..C26 plane	0.038(1)	0.182(2)	0.047(1)	0.637(3)
dist of V2 from C31..C36 plane	0.405(1)		0.035(1)	
dist of V2 from C41..C46 plane	0.056(1)		0.045(1)	
dist of V2 from C51..C56 plane	0.113(1)		0.107(1)	
Dihedral Angles between Mesityl Rings (deg)				
C1..C6 ∧ C11..C16	80.6(1)	82.1(5)	85.2(2)	83.5(3)
C1..C6 ∧ C21..C26	66.4(1)	67.0(3)	66.7(2)	81.6(3)
C11..C16 ∧ C21..C26	71.2(1)	70.5(4)	53.0(2)	70.5(3)
C31..C36 ∧ C41..C46	82.2(1)		62.7(2)	
C31..C36 ∧ C51..C56	67.3(1)		67.8(2)	
C41..C46 ∧ C51..C56	89.5(1)		88.2(2)	
Dihedral Angles between the Mesityl Rings and the Basal Coordination Plane (deg)				
C1..C6 ∧ C1,C11,C21	36.0(1)	75.3(4)	84.4(2)	57.8(3)
C11..C16 ∧ C1,C11,C21	79.5(1)	75.7(5)	34.4(2)	65.2(3)
C21..C26 ∧ C1,C11,C21	38.0(2)	11.3(4)	24.2(2)	24.5(3)
C31..C36 ∧ C31,C41,C51	85.4(2)		25.8(2)	
C41..C46 ∧ C31,C41,C51	43.5(1)		63.6(2)	
C51..C56 ∧ C31,C41,C51	16.9(1)		18.4(2)	
Relevant Torsion Angles between Mesityl Rings (deg)				
C6−C1..C11−C12	30.9(4)	−0.1(13)	−22.2(7)	−18.0(11)
C2−C1..C11−C16	27.4(4)	2.0(13)	−28.1(7)	−24.2(9)
C46−C41..C51−C52	28.0(4)		−17.7(7)	
C42−C41..C51−C56	29.2(5)		−21.2(7)	
(b) Within the Dimeric $[\{V(Mes)_3\}_2$-μ-$(N_2)]$ Unit				
Relevant Torsion Angles (deg)				
C21−V1..V1′−C21′		180.0(−)		−28.7(4)
C21−V1..V2..C31	168.3(2)		−160.8(2)	
Relevant Dihedral Angles (deg)				
C21..C26 ∧ C21′..C26′		180.0(−)		24.5(3)
C21..C26 ∧ C31..C36	38.0(2)		24.2(2)	

[a] Prime denotes a transformation of $1 - x, -y, 1 - z$ and $-x, y, -0.5 - z$ for **12** and **14**, respectively.

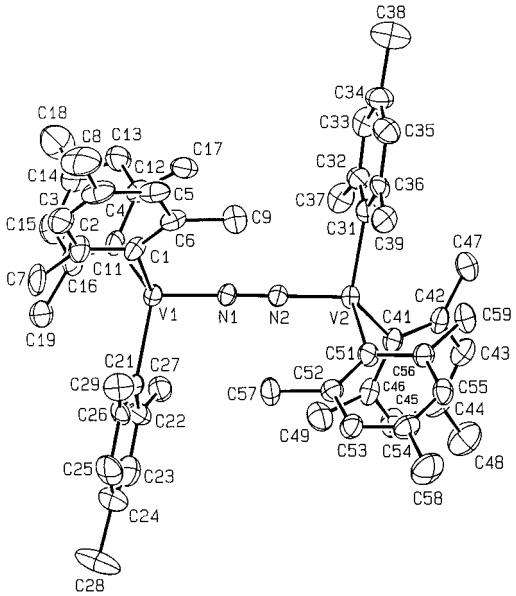

Figure 3. ORTEP drawing of the anion in complex **13** (25% probability ellipsoids).

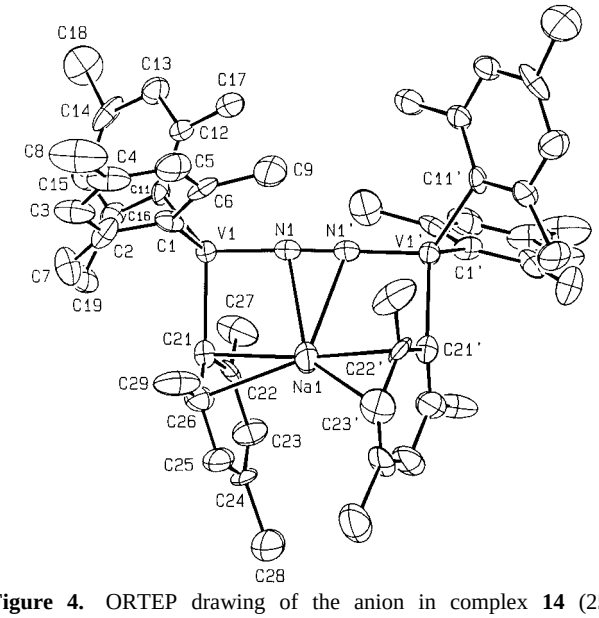

Figure 4. ORTEP drawing of the anion in complex **14** (25% probability ellipsoids). Prime denotes a transformation of $-x, y, 0.5 - z$. The disorder involving Na1 has been omitted for clarity.

normal to the mean basal plane is 15.1(3)°. Two symmetry related mesityl ligands (C21···C26) in a dimer face each other [dihedral angle 24.5(3)°] to provide a cavity which accommodates a sodium cation (disordered over two positions about the 2-fold axis) which in turn gives rise to a sandwich-type compound. The trend of the Na1···C distances involving the carbon atoms suggests a η^2 sodium−mesityl and η^3 sodium−mesityl for the C21−C26 and C21′−C26′ mesityl rings, respectively (and *vice versa* for the Na1′ cation) (Table 4). Other Na1···C contacts are longer than 2.93 Å.[21] In addition the alkali metal η^2 interacts with the dinitrogen molecule [Na1−N1, 2.513(12); Na1−N1′, 2.607(12) Å] probably giving rise to a significant lengthening of the N−N bond distance with respect to the values found in **11**, **12**, and **13** where this kind of

interacion is not present. The V−C bond distances are longer than those observed in **1**[8a] as a consequence of the presence of the V−N multiple bond. They are in agreement with those found in complex **13**. The large displacement of vanadium from the plane of the C21···C26 aromatic ring is consistent with the pyramidal nature of the C21 carbon atom induced by the interaction with the sodium cation. The distance of C21 from the plane through the three bonded atoms is 0.156(9) Å. The mutual orientation of the mesityl rings in the two $[V(Mes)_3]$ units is mainly determined by the inclusion of the Na^+ cation, as can be seen from the appropriate conformational parameters properly given in Table 3. The two $[V(Mes)_3]$ units in a dimer are arranged in such a way as to put two rings approximately parallel to each other: C21···C26 and C21′···C26′ for **12** and **14**; C21···C26 and C31···C36 for **11** and **13**. The two parallel rings are *cis*-oriented in complex **14** and *trans*-oriented in complexes **11**−**13** with respect to the V···V line, as indicated by the values of the C−V···V−C torsion angles (Table 5). Within each $V(Mes)_3$ unit the orientation of the mesityl rings is given by the dihedral angles between mesityl rings and between the mesityl rings and the coordination plane (Table 5). In spite of the rather low accuracy of the X-ray analysis we can make the following observations: (i) the geometry of the molecule is similar to that observed in complexes **11** and **13**; the values of the V−C bond distances [average 2.124(9) Å] are midway between those observed in complexes **11**, **13**, and **14** and are in agreement with those found in the neutral $[V(Mes)_3(THF)]$[8a] starting molecule (Table 5); (ii) the range of the K−C_{mes} distances in complex **12** suggest η^6 interactions involving the potassium cation and the two eclipsed mesityl rings.[20] Such an interaction is almost usual. In Table 5 we report the comparison between the most important conformational parameters related to complexes **11**−**14**. These data show that the interaction of the alkali cation with the dinuclear skeleton is almost ineffective for the general conformation of the dimeric complexes.

The structural parameters for the V−N−N−V skeleton (Tables 3−5) are extremely close in all four complexes regardless of the overall charge of the complex, the oxidation state of the metal or the reduction degree of N_2, and the binding (or not) of the alkali cation within the dimeric framework. The V−N−N−V skeleton is linear, with a V−N bond distance ranging from 1.744(6) to 1.770(3) Å and a N−N length varying from 1.222(4) to 1.271(8) Å.[5] These data, while not providing any criteria for the reduction degree of N_2 or its activation toward electrophiles, allow us to draw the [V═N═N═V] cumulene structure for the V_2N_2 skeleton.

C. Electrochemistry. This section reports the electrochemical behavior of **1** under argon and dinitrogen. The numbering scheme is that shown in Schemes 2, 3, and 5. We will assume that, since the solvent is THF, the naked anions **7** and **8** shown in Scheme 2 form from **11**−**14** dissolved in THF.

Figure 5a shows the cyclic voltammetric (CV) response of a THF solution of **1** at a Pt electrode under argon. A single-oxidation process is displayed in the anodic window (peak couple A/B) at $E^{\circ\prime} = +0.16$ V vs SCE. The electrochemical parameters for the A/B couple in the scan rate (υ) range 0.05−50 V s^{-1} are the following: (i) i_p vs $\upsilon^{1/2}$ plots for both peaks are linear through the origin, indicating diffusion-controlled and adsorption-free processes;[21] (ii) ΔE_p is constantly 70 mV when corrected by comparison with the behavior of the ferrocene/ferrocenium (Fc/Fc^+) couple (added as an internal standard); moreover ($E_p - E_{p/2}$) values of both peaks are constantly 65 mV, near the theoretical expectation for a 1e E_{rev} process[21] (these data are consistent with a Nernstian (electrochemically reversible) process); (iii) $i_{pc}(B)/i_{pa}(A)$ ratio increases from 0.83 to 0.93 as the sweep rate increases; furthermore $E_p(A)$ vs log υ plot is linear with a slope of 5 mV. These features are consistent with a chemically almost reversible 1e oxidation process.[21]

Scheme 5. Proposed Mechanism for the Electrochemical Reduction of 1 under N_2

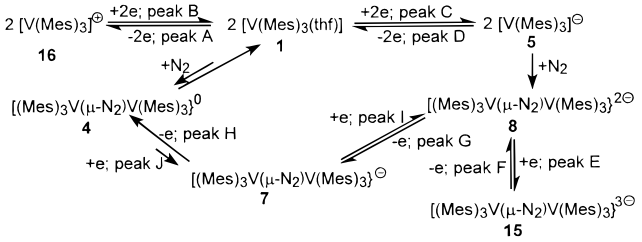

This behavior can be easily interpreted as a metal-centered oxidation from $[V(Mes)_3]$ to $[V(Mes)_3]^+$, **16** (see Scheme 5), though the process is certainly not involved in the N_2-reduction pattern.

The cathodic sweep shows a well-behaved peak couple (C/D) at $E^{\circ\prime} = -2.09$ V. The electrochemical parameters, in the scan rate range 0.05−50 V s^{-1} are the following: (i) i_p vs $\upsilon^{1/2}$ plots for both peaks are linear through the origin; (ii) ΔE_p varies from 83 to 140 mV, even when corrected by comparison with the behavior of the Fc/Fc^+ couple; moreover ($E_p - E_{p/2}$) values of both peaks increase from 70 to 120 mV as the sweep rate increases; (iii) $i_{pa}(D)/i_{pc}(C)$ ratio is unity, and $E_p(C)$ vs log υ plot is linear with a slope of 25 mV.

All these data are consistent with a 1e electrochemically semireversible and chemically reversible reduction process from **1** to $[V(Mes)_3]^-$, **5** (Schemes 2 and 5). Some geometrical rearrangements should occur in **5**, if one attaches structural significance to the moderate rate of the observed charge transfer.[19] However, there is no evidence of $[V(Mes)_4]^-$ anion formation during such experiments. Indeed, an authentic sample of **9** (Figure 5a) shows a fully reversible oxidation process (peak couple A′/B′) at $E^{\circ\prime} = +0.68$ V, very far from the A/B couple of **1**. Therefore, in the short CV time scale the evolution from **5** to $[V(Mes)_4]^-$, **9**, does not occur. This would require, as in the much slower chemical reduction, the presence of unreacted **1** (see Scheme 3).

If N_2, instead of Ar, is bubbled, the cathodic scenario modifies as shown in Figure 5b. A new peak system E/F appears at a more cathodic potential ($E^{\circ\prime} = -2.40$ V), together with two reoxidation peaks G ($E_p = -1.79$ V) and H ($E_p = -0.95$ V) (both evaluated at 0.2 V s^{-1} scan rate). Peaks G and H are unambiguously related to the C/D system: their appearance corresponds to a decrease of the peak D current, and when the sweep is reversed at $E_\lambda = -2.30$ V (so eliminating the electrogeneration of couple E/F), both are still present in similar intensity. Moreover, if we impose a vertex delay of 5 s at $E_\lambda = -2.30$ V, peaks G and H both increase with respect to peak D. Reoxidation peaks G and H as well as the peak couple E and F disappear at scan rates as high as 5 V s^{-1}. Therefore, the increase of scan rates (which quenches ensuing chemical reactions) restores a CV response identical to that obtained under the Ar atmosphere. These extra peaks represent electrochemical processes corresponding to different species slowly generated from **5**. A multiscan CV experiment, traversing peak H, shows

(20) Weiss, E. *Angew. Chem., Int. Ed. Engl.* **1993**, *32*, 1501.

(21) (a) Bard, A. J.; Faulkner, L. L. *Electrochemical Methods*; Wiley: New York, 1980. (b) Brown, E. R.; Sandifer, J. R. In *Physical Methods of Chemistry*; Rossiter, B. W., Hamilton, G. F., Eds; Wiley: New York, 1986; Vol. II, Chapter IV. (c) Adams, R. N. *Electrochemistry at Solid Electrodes;* Marcel Dekker: New York, 1971. (d) Heardridge, J. B. *Electrochemical Techniques for Inorganic Chemists;* Academic: London, 1969.

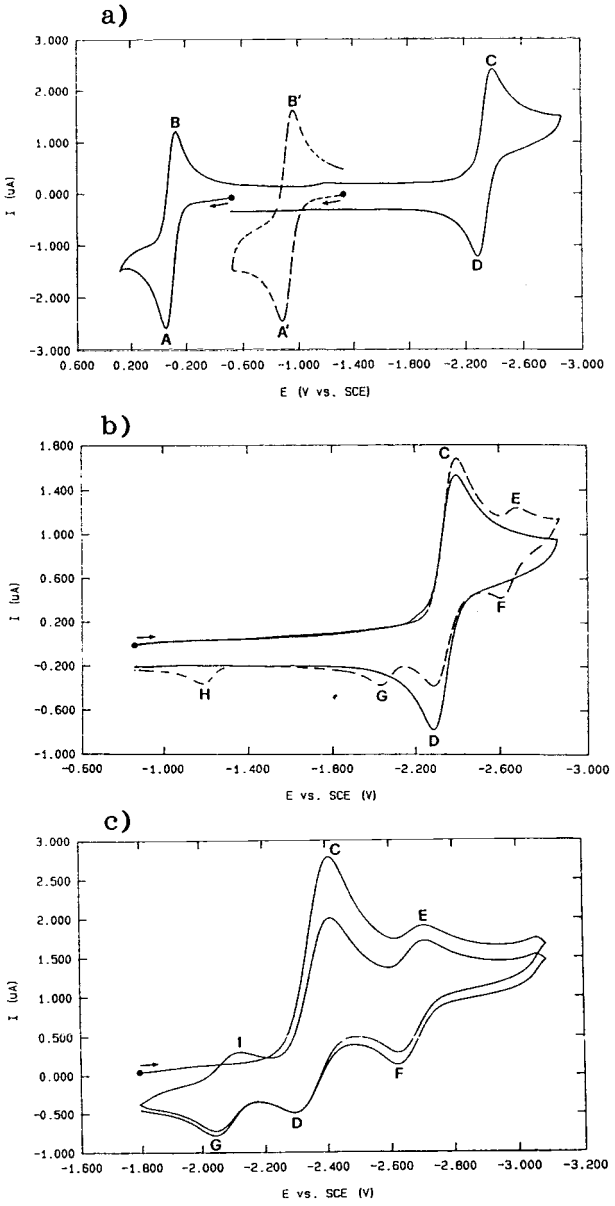

Figure 5. (a) CV responses of THF solutions of **1** (solid line) and **9** (dashed line), containing $NaBPh_4$ (0.2 M) as supporting electrolyte at a Pt electrode, under Ar, $\upsilon = 0.2$ V s^{-1}, (●) starting potentials. (b) CV responses of a THF solution of **1** under Ar (solid line) and under N_2 (dashed line), $\upsilon = 0.2$ V s^{-1}, (●) starting potential. (c) Multiscan CV response of a THF solutions of **1** under N_2, $\upsilon = 0.2$ V s^{-1}, (●) starting potential.

no difference in the number of peaks and relative intensities in the successive cathodic sweeps. This seems to indicate that only the reoxidation process at peak H regenerates neutral **1** in almost quantitative yield, in spite of the cascade of electrochemically induced transformations. On the contrary, if the reoxidation sweep is stopped before traversing peak H (E_λ = −1.55 V), a new peak I (clearly related to peak G) appears at E_p = −1.88 V (0.2 V s^{-1}), and the intensities of peak C considerably decrease (Figure 5c), indicating that part of **1** has been subtracted to the diffusion layer. In these experimental conditions one can observe three reversible peak systems at $E^{o\prime}$ = −1.84 V (G/I), −2.10 V (C/D) and −2.40 V (E/F) (Figure 5c).

Controlled-potential coulometry at a platinum gauze (E_w = −2.30 V) consumes 1e per molecule of **1**, with a concomitant color change from blue to dark brown. The CV response of the exhaustively reduced solution (Figure 6a) gives a response

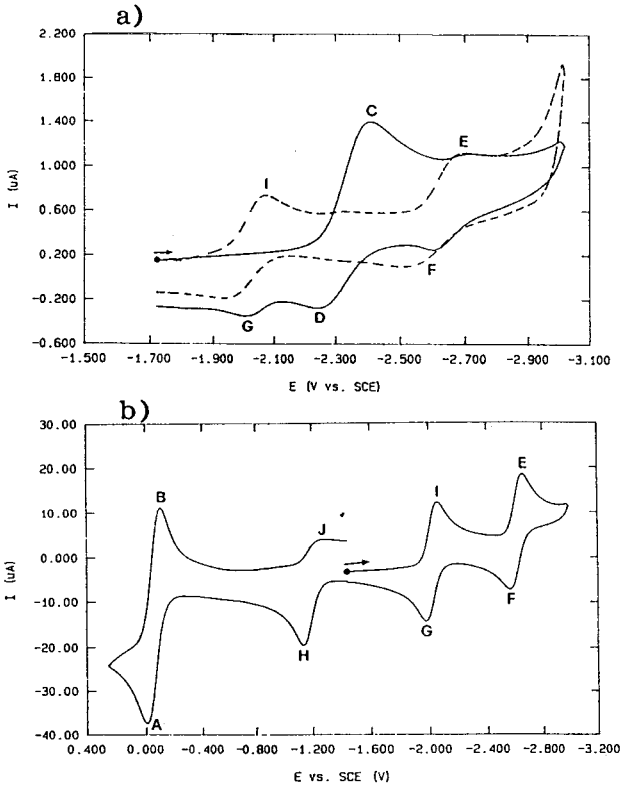

Figure 6. (a) CV responses of a THF solution of parent complex **1** (solid line) and of the resulting solution after exhaustive electrolysis at E_w = −2.30 V under N_2, $\upsilon = 0.2$ V s^{-1}. (b) CV response of a THF solution of **7** (**11**) under N_2, $\upsilon = 0.2$ V s^{-1}, (●) starting potential.

similar to that of Figure 5c. Noteworthy, the intensity of peak I is about half (47%) of the initial peak C, suggesting that it is related to a dimer.

Variations of E_p(C) have been examined both as a function of scan rate and concentration (c) of **1**. Logarithmic analysis of E_p(C) as a function of υ have been performed in concentrations of **1** ranging from 1 to 4 mM. An average value of 24 mV/decade is obtained for the slope of $\delta E_p/\delta(\log \upsilon)$, whereas a negligible value is obtained for the slope of $\delta E_p/\delta(\log c)$. The observed variation of E_p(C) with log υ is in agreement with a dimerization mechanism, but the very small variation of E_p(C) with log c apparently contradicts this interpretation.[21] However, on the basis of the chemical results and the following tests on the model compound **7**, N_2 must plays an important role in such a dimerization process. Its concentration after saturation of THF solvent is very low, and this can represent a limiting factor. In conclusion (see Scheme 5), the primary reduction product **5** reacts with nitrogen to afford $[(Mes)_3V-N_2-V(mes)_3]^{2-}$, **8**. This complex can be reversibly reduced in CV time scale to **15**. However, controlled-potential coulometry at a platinum gauze (E_w= −2.70 V) causes total decomposition of the complex as can be seen by the disappearance of CV peaks.

Further evidence of the original dimerization is provided by comparing the previous electrochemical results with that of an authentic sample of $[(Mes)_3V(\mu\text{-}N_2)V(Mes)_3]^-$, **7**, in the form of **11**. Two reduction processes (Figure 6b) are present in the cathodic sweep corresponding to the peak couples I/G and E/F. The peak−current ratio of these reductions, namely, $[i_{pc}(I)/i_{pc}(E)]$, is 1:1. When the anodic sweep is analyzed, the passage through the oxidation peak H (having the same current intensity as peaks I and F) causes the regeneration of **1**, as previously shown. **1** can be further oxidized at peak A; interestingly the ratio of the previously observed peaks (namely, I, E, and H) with respect to this 1e oxidation is 1:2. This feature unambigu-

Table 6. Redox Potentials (V vs SCE) for the Complexes under Study in THF Solution (0.2 M $NaBPh_4$) at a Pt Electrode

	peaks				
compd	A/B[a]	C/D[a]	E/F[a]	G/I[a]	H[b]
1	+0.16	−2.09	−2.40	−1.84	−0.95
solution after reduction of **1**			−2.40	−1.80	−0.94
7 (**11**)	+0.16		−2.37	−1.79	−0.92

[a] $E^{o\prime} = (E_{pa} + E_{pc})/2$. [b] E_p evaluated at 0.2 V s^{-1}.

ously demonstrates that all the species associated at the peak couple I/G, E/F, and H/J are in dimeric forms. The electrochemical parameters for the I/G and E/F couples are consistent with diffusion-controlled, chemically and electrochemically reversible 1e/molecule reduction processes. On the contrary, the $[i_{pc}(J)/i_{pa}(H)]$ ratio is always less than unity (namely, it varies from 0.3 to 0.7 in the scan rate range 0.05−50 V s^{-1}) showing that the $[(Mes)_3V(\mu\text{-}N_2)V(Mes)_3]$, **4**, (Scheme 5) releases N_2 back to **1** in the presence of THF.

Table 6 summarizes the electrochemical data.

The proposed mechanism of the electroreduction of **1** in the presence of nitrogen is summarized in Scheme 5. The intimate mechanism of the dimerization process (a key step for N_2-activation) has not been completely elucidated on the basis of the electrochemical experiments. The paramount step seems to be the coupling between two **5** anions.

The distinctive characterstics of the chemical and electrochemical reduction of **1** in the presence or absence of N_2 should be commented on at this stage. The striking difference between the two is the much faster electrochemical reduction, compared with the chemical one, of $[V(Mes)_3(THF)]$, **1**, to $[V(Mes)_3]^-$, **5**. Remember that both the ligand disproportionation reaction (Scheme 3) and the formation of **7** require the simultaneous presence of **1** and **5**. It is for this reason that the electrochemical reduction of **1** under Ar does not result in the formation of $[V(Mes)_4]^-$. However, while under N_2 the primary compound formed is not **7**, but **8**, a consequence of the reaction of **6** with **5**. In the much slower chemical reduction the formation of **7** accounts for the presence of **1** reacting with **6**.

D. Magnetic Properties and Theoretical Calculations. Magnetic susceptibilities data for complexes **11**−**13** and **4** were collected with a SQUID magnetometer in the temperature range 1.9−300 K and are displayed in Figures 7 and 8. The data for **14** are not reported as they are practically coincident with those for **13**.

We see that for **11**−**14** the magnetic moment per vanadium is essentially constant down to low temperatures, with a value of about 1.7 μ_B for complexes **12**−**14** and 1.3 μ_B for complex **11**. In complex **11** there is only one spin center per dimer so that the magnetic moment can be simply fitted with a Curie spin-only formula[22] giving $g = 2.09$. For complexes **13** and **14** the magnetic data are accounted for with two independent $S = {}^1/_2$ spin centers on the two metals (giving $g = 1.96$ and $g = 1.95$, respectively) while for **12** the data can be fitted with the simple Bleany−Bowers equation[23] obtained, assuming that the interaction between the two spin centers were described by the Heisenberg spin Hamiltonian $H = -2JS_1 \cdot S_2$, considering a pair of exchange-coupled ions with $S_1 = S_2 = 1/2$. The best fit to the collected data yielded $g = 2.06$, $J = -0.65$ cm^{-1}. These results indicate a negligible or very small antiferromagnetic coupling between the two S=1/2 spin centers through the N−N bridge.

In terms of the energy level pattern the results above indicate that for complexes **13**−**14** the lowest states are two perfectly degenerate singlet and triplet, for complex **12** the ground state is a singlet with a triplet only 1.3 cm^{-1} above, and for complex **11** the ground state is a well-isolated doublet.

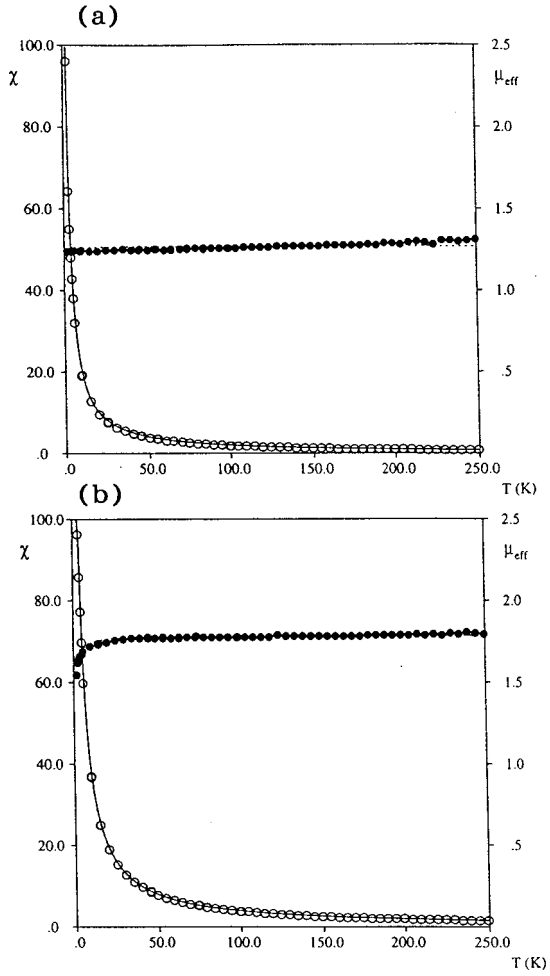

Figure 7. Magnetic susceptibility (○; 10^{-3} cm^3 mol^{-1}) and effective magnetic moments (●; BM) *per* vanadium *vs* temperature for complex **11** (a) and complex **12** (b).

A completely different behavior has been observed for **4**, for which the magnetic moment shows a steady decrease from 1.2 μ_B at 300 K to 0.2 μ_B at 1.9 K (Figure 8b). A careful analysis of the temperature dependence of the magnetic susceptibility reveals that such behavior is essentially due to a large temperature independent paramagnetism (TIP) and a good fit is actually obtained for $N\alpha = 1.2 \times 10^{-3}$ including the presence of an almost negligible amount, <0.1%, of monomeric V(III) impurities. Such magnetic behavior indicates an isolated nonmagnetic singlet ground state, the large TIP being due to the presence of a low-lying (but thermally nonpopulated) triplet state (presumably around 1000−2000 cm^{-1} or higher).[24]

Such observed magnetic behaviors are inconsistent with pairs of d^3−d^3 (complexes **12**−**14**) or d^2−d^3 (complex **11**) ions, corresponding to V(II)−V(II) and V(III)−V(II) formal oxidation states of the metals, respectively. Rather they indicate pairs of d^1−d^1 or d^0−d^1 ions, suggesting a change in the oxidation states of vanadium atoms, respectively, to V(IV)−V(IV) or V(V)−V(IV), with a corresponding four-electron reduction of the dinitrogen moiety. The magnetic behavior of **4** could, instead, be interpreted as due to a very strong antiferromagnetic interaction within a pair of d^2−d^2 ions, which leaves an isolated singlet state.

(22) Carlin, R. L. *Magnetochemistry*; Springer: Berlin, Germany, 1986.
(23) O'Connor, C. J. *Progr. Inorg. Chem.* **1982**, *29*, 203.
(24) Kahn, O. *Molecular Magnetism*; VCH: Weinheim, Germany, 1983.

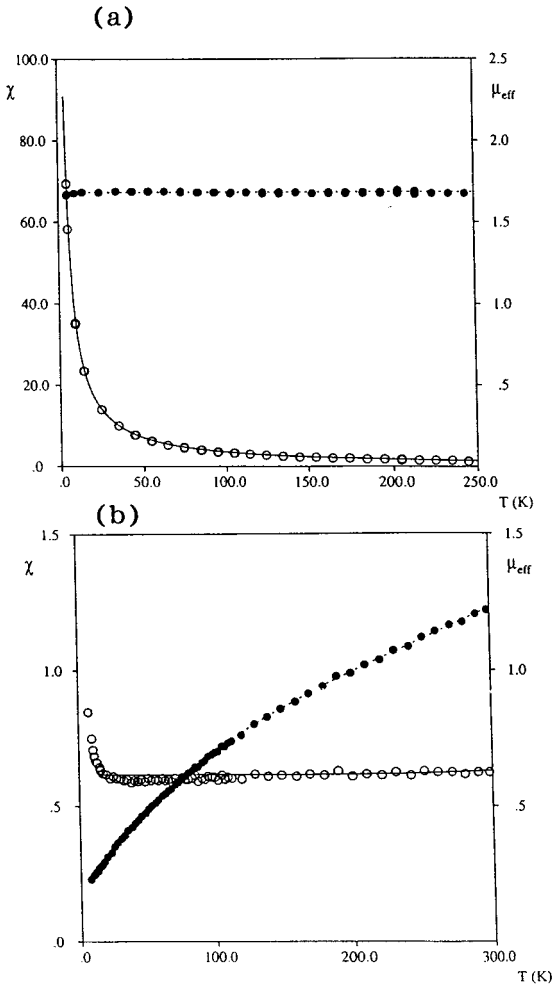

Figure 8. Magnetic susceptibility (○; 10^{-3} cm^3 mol^{-1}) and effective magnetic moments (●; BM) *per* vanadium *vs* temperature for complex **13** (a) and complex **4** (b).

Scheme 6

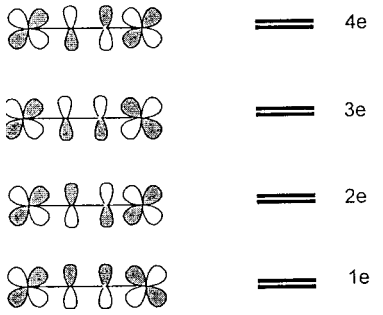

These magnetic behaviors can be better rationalized on the basis of the overall electronic structure of the considered dinuclear complexes. A qualitative description of bonding in metal dinitrogen complexes is based on the four-center four-orbital interaction scheme for the MNNM linear moiety reported in Scheme 6.[25]

There are two sets of these four-center molecular orbitals which are obtained by the linear combinations of the two sets of mutually orthogonal d_π (M) and p_π (N) atomic orbitals. As an overall result, there will be four doubly degenerate energy levels with energies increasing with the nodal number of the molecular orbitals and which are designated 1e, 2e, 3e, 4e. The scheme is completed by four δ type orbitals (usually designated as $1\delta - 4\delta$ and lying between 2e and 4e), built by the bonding and antibonding combinations of the d_δ metal orbitals which do not interact with any dinitrogen orbital. These orbitals are to be filled with four electrons from the N_2 moiety and $n + m$ electrons from the two metal fragments (assumed with formal d^n and d^m configurations). The strengths of the M−N and N−N bonds are determined by the occupancies of the 2e and 3e levels. The 2e level has π^*(N−N) character and its population results in a relevant decrease of the N−N bond order while the 3e orbital has a π(N−N) character and its population results in an increase of the N−N bond order. Most of the qualitative[26−29] and semiempirical[30−32] descriptions of the metal dinitrogen bonding in dinuclear N_2-bridged complexes have been performed on the basis of this model. Most of them generally agree that the best electron count for dinitrogen activation corresponds to two d^2 metal fragments.

Scheme 7

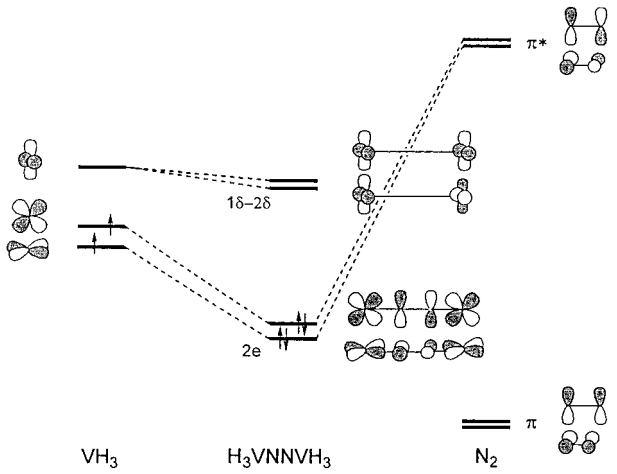

We have recently performed *ab initio* calculations on a series of $[\{VH_3\}_2(\mu\text{-}N_2)]^q$ ($q = 0, -1, -2$) complexes of C_{2v} symmetry as simplified models of **4** and **11**−14,[33] interpreting the results in terms of the four-center model. Some of those results will now be used to interpret the magnetic behavior and the extent of dinitrogen activation in such complexes. The calculated energy ordering and nature of the main frontier molecular orbitals is shown in Scheme 7, where we report the occupancy for **4**. There are two sets of almost doubly degenerate orbitals.

The two highest occupied orbitals correspond to the 2e level while the two lowest unoccupied orbitals, about 1 eV higher in energy, are mostly metal orbitals of d_δ character. The 3e level has been found to be far higher in energy, while the 1e level is low-lying and essentially of π(N−N) character. In **4**, the 2e set is filled by two d electrons from each $V(Mes)_3$ metal fragment (formally d^2) and a singlet ground state is found. However, the gap between the 2e and $1-2\ \delta$ sets of

(25) Chatt, J.; Fay, R. C.; Richards, R. L. *J. Chem. Soc. A* **1971**, 2399. Treitel, J. M.; Flood, M. T.; March, R. E.; Gray, H. B. *J. Am. Chem. Soc.* **1969**, *91*, 6512. Treitel, J. M.; Flood, M. T.; March, R. E.; Gray, H. B. *J. Angew. Chem., Int. Ed. Engl.* **1974**, *13*, 639.

(26) Sunner, R. D.; Manriquez, J. M.; Marsh, R. E.; Bercaw, J. E. *J. Am. Chem. Soc.* **1976**, *98*, 8351.

(27) Sunner, R. D.; Duggan, D. M.; McKenzie, T. C.; Marsh, R. E.; Bercaw, J. E. *J. Am. Chem. Soc.* **1976**, *98*, 8358.

(28) O'Regan, M. B.; Liu, A. H., Finch, W. C.; Schrock, R. R.; Davis, W. M. *J. Am. Chem. Soc.* **1990**, *112*, 4331.

(29) Kol, M.; Schrock, R. R.; Kempe, R.; Davis, W. M. *J. Am. Chem. Soc.* **1994**, *116*, 4382.

(30) Pelican, P.; Boca, L. *Coord. Chem. Rev.* **1984**, *55*, 55.

(31) Powell, C. B.; Hall, M. B. *Inorg. Chem.* **1984**, *23*, 4619.

(32) Goldberg, K. I.; Hoffmann, D. F.; Hoffmann, R. *Inorg. Chem.* **1982**, *21*, 3863.

(33) Re, N.; Rosi, M.; Sgamellotti, A.; Floriani, C.; Solari, E. *Inorg. Chem.* **1994**, *33*, 4390. Re, N.; Rosi, M.; Sgamellotti, A.; Floriani, C. *Inorg. Chem.* **1995**, *34*, 3410.

orbitals is not very high so that the triplet excited state (although not populated) is sufficiently low to give a high second-order contribution to magnetic susceptibility. In **11**, one more electron must be put in the δ orbital and the ground state is a well-isolated doublet. In **12**−**13**, two more electrons occupy the two degenerate δ orbitals. Taking into account that the δ orbitals have no contribution from the bridging dinitrogen ligand, such a $(1\delta)^1(2\delta)^1$ configuration physically corresponds to a neglegible antiferromagnetic interaction between two formally d^1 metal centers consistent with the observed magnetic behavior. Our previous calculations[33] gave a triplet ground state. However, we should consider that an SCF approac h is inappropriate for this situation[24] and favors the high spin states.

On the basis of this orbital scheme some considerations can be made on the nature of the metal−dinitrogen bonding. In all the considered complexes, the 2e level is occupied and the 3e level is empty, so that a marked activation of dinitrogen would be expected. However, a much lower activation is observed for **4**. This can be explained by taking into account that dinitrogen activation depends not only on the occupancy of the 2e and 3e levels but also on the extent of metal−nitrogen mixing in these orbitals. In particular, the mixing in the 2e level is determined by the energy difference between the d_π orbitals of the metal fragments and the empty π^* orbitals of N_2. The higher the metal orbitals are, the higher π^*(N−N) character the 2e level has, i.e., a higher reduction of the N−N bond order is expected. The d orbital energies in $[V^{II}(Mes)_3]^-$ metal fragments are considerably higher than those in $[V^{III}(Mes)_3]$ fragments (V(II) is a much better π donor than V(III)) so that a higher dinitrogen activation is expected for **12**−**14** with respect to **4**, as observed. An intermediate situation is expected and found for the mixed valence species **11**. The *ab initio* calculations of ref 33 confirmed these forecasts; a small π^*-(N−N) contribution was calculated for the 2e orbitals of **4** and increasingly higher contribution for **11** and **12**−**14**.

Conclusions

This is a rather unique case in which the dinitrogen molecule bridging two metal centers has been subjected to a controlled stepwise chemical and electrochemical reduction going from $[(Mes)_3V(\mu\text{-}N_2)V(Mes)_3]$, **4**, to $[(Mes)_3V(\mu\text{-}N_2)V(Mes)_3]^-$, **7**, and then to $[(Mes)_3V(\mu\text{-}N_2)V(Mes)_3]^{2-}$, **8**, that is from an inactive to reactive reduced form. We have to emphasize a quite remarkable effect as a consequence of the addition of a single electron to **4**. This does not cause a monoelectronic reduction of N_2, but instead induces the dimetallic unit to promote a multielectronic reduction of dinitrogen in **7**, and consequently in **8**. This has been expressed by writing down the cumulene structures for **7** and **8**, as supported by the structural analysis on **11**−**14**. In addition, the magnetic and theoretical studies support the formulation of a d^2−d^2 couple in the case of **4**, a d^1−d^0 and a d^1−d^1 in the case of **7** and **8** , respectively, with the effective reduction of the dinitrogen molecule. This has been chemically revealed in the protonation reaction leading to NH_3 and N_2H_4 in the case of **7** and **8**.

Acknowledgment. We thank the Fonds National Suisse de la Recherche Scientifique (FNS, Bern, Switzerland, Grant No. 20-40268.94), Ciba Specialty Chemicals (Basel, Switzerland), and the Centro Nazionale delle Ricerche (CNR, Rome, Progetto Bilaterale Italia/Svizzera) for financial support; Dr. Lubomir Pospisil (Academy of Science of the Czech Republic, Praha) is also acknowledged for stimulating discussion.

Supporting Information Available: Supplementary drawings (Figures S1−S4), tables of experimental details associated with data collection and structure refinement (Table S1), atomic coordinates (S2−S9), anisotropic thermal parameters (S10−S13), bond lengths and bond angles (S14−S17), and details of X-ray crystallography for **11**−**14** (34 pages). Ordering information is given on any current masthead page.

JA971229Q